NREL/TP-442-5619 • UC Category: 261 • DE93010032

Defining the Normal Turbine Inflow Within a Wind Park Environment

Neil D. Kelley

Prepared for the
IEA Topical Meeting 24—Wind
Conditions for Wind Turbine Design
April 29–30, 1993
Roskilde, Denmark

National Renewable Energy Laboratory
1617 Cole Boulevard
Golden, Colorado 80401-3393
Operated by Midwest Research Institute
for the U.S. Department of Energy
under Contract No. DE-AC02-83CH10093

Prepared under Task No. WE318010

June 1993

NOTICE

Printed in the United States of America
Available from:
National Technical Information Service
U.S. Department of Commerce
5285 Port Royal Road
Springfield, VA 22161

Price: Microfiche A01
Printed Copy A03

Codes are used for pricing all publications. The code is determined by the number of pages in the publication. Information pertaining to the pricing codes can be found in the current issue of the following publications which are generally available in most libraries: *Energy Research Abstracts (ERA)*; *Government Reports Announcements and Index (GRA and I); Scientific and Technical Abstract Reports (STAR)*; and publication NTIS-PR-360 available from NTIS at the above address.


Printed on recycled paper

IEA Annex XI
Expert Meeting 24, *Wind Conditions for Turbine Design*
Risø, April 29-30, 1993

DEFINING THE NORMAL TURBINE INFLOW WITHIN A WIND PARK ENVIRONMENT

N. D. Kelley
Wind Technology Division
National Renewable Energy Laboratory
Golden, Colorado U.S.A.

Introduction

This brief paper discusses factors that must be considered when defining the "normal" (as opposed to "extreme") loading conditions seen in wind turbines operating within a wind park environment. We define the "normal" conditions to include fatigue damage accumulation as a result of

- *start/stop cycles*
- *emergency shutdowns*
- *the turbulence environment associated with site and turbine location.*

We also interpret "extreme" loading conditions to include those events that can challenge the survivability of the turbine.

Loading Characteristics Responsible for Maximum Fatigue Damage Accumulation

Recent analyses of the loading events associated with turbine rotor blades constructed of composite materials have shown that the bulk of the fatigue damage is associated with infrequent (or low-cycle), high-amplitude (peak-to-peak load) events. This is particularly true of blade materials that are characterized by a high S-N exponent.

We recently analyzed two sets of extensive root flapwise bending moment measurements taken from two stall-controlled, rigid-hub Micon 65 turbines and an NPS-100 teetered-hub turbine. The blades of these rotors were of similar length and weight. We used rainflow counting to determine the alternating (p-p) stress cycle distributions seen by these three machines over record lengths of 67.5 and 70.1 hours, respectively, in wind park environments. Figure 1 compares the results for the rigid and teetered rotors. The maximum cyclic stress reduction for the teetered rotor occurs near 15 kNm but asymptotically approaches the rigid ones at both the high- and low-cycle extremes. Above a p-p value of 15 kNm, both hub designs exhibit a decaying exponential distribution, as is indicated in the figure.

The region of the curves of Figure 1 above p-p values of 15 kNm is the greatest concern from the viewpoint of fatigue damage accumulation. It is therefore very important, when defining the "normal" loading environment for a wind park, to identify such low-cycle events and include them in any dynamic simulations.

Impact of Coherent Turbulent Structures

The consequences of a turbine rotor blade encountering a coherent or organized patch of turbulence are demonstrated in Figures 2 and 3. Figure 2 plots the root edgewise bending moments from Blade No. 1 of two, side-by-side, Micon 65 turbines. One of the turbines had blades based on the NREL (SERI) thin airfoil family and the other with refurbished, original-equipment AeroStar blades. Also presented are the root flapwise bending moments of the three blades on the AeroStar-equipped turbine. The plots indicate that the AeroStar rotor reacted differently to an excitation that lasted approximately 3-4 seconds.

The corresponding hub-height turbulent inflow characteristics are presented in Figure 3. Figure 3a shows the strong correlation of the instantaneous $u'w'$ and $v'w'$ shear or Reynolds stresses within the period of enhanced blade response. The estimated hub-elevation vorticity components (ω_i) and helicity ($\mathbf{u}_i\omega_i$) time series are plotted in Figure 3b. These parameters indicate the existence of a vortical structure that could be responsible for the shear stress pattern in Figure 3a. The evidence implies a one-to-one correspondence between the enhanced cyclic activity on Blade No.1 of the AeroStar rotor and the presence of a vortical structure in the inflow.

We examined the inflow conditions associated with the largest observed root flapwise tension peak and one of the larger compression (negative) ones. Figure 4a plots a five-second record of the flapwise loads from each of the three blades on the NREL rotor. The largest excursion occurs on Blade No. 3. The remaining two blades also are affected but to lesser degrees perhaps indicating that a coherent structure is convecting through the rotor disk. The enhanced loading extends to a period of about 2 seconds. The corresponding hub-height estimated vorticity/helicity record also lasts about the same amount of time. When the later is aligned with the Blade No. 3 peak of Figure 4a, the plot of Figure 4b results. Similarly, Figure 5a documents the peak compression load experienced by Blade No. 2. Again, the corresponding vorticity/helicity record is superimposed in Figure 5b, *but no time alignment has been performed.* The plots of Figures 4 and 5 do seem to support the hypothesis that organized, vortical structures are indeed connected with large induced blade stresses.

We looked more closely at the population of inflow conditions connected with the 25 largest flapwise stress cycles seen on either of the two Micon 65 rotors. In applying damage theory, it is assumed that the rotor materials have an *infinite memory.* This requires that all cycles must be closed to assess the corresponding damage. When the entire 67.5-hour record was rainflow counted as a single time series, a significant number of large-amplitude cycles were found that spanned the original ten-minute records. Figure 6 plots the largest maximum and minimum pairing found in the data set from the NREL-equipped rotor. The period between the minimum (compression) and positive (tension) peaks was 43 hours or almost three days. From a meteorological point of view, the conditions associated with each of the peaks can be considered *independent events*. Thus, we can look at the meteorological conditions associated with the population of the peak tension and compressional stress events independently also. We did that and found the following:

- ***All** of the tension peaks associated with the largest stress cycles occurred during slightly stable flows emerging from a deep canyon southwest of the wind park.*
- *The common time of occurrence was 22 h local standard time.*
- *The negative (compression) peaks of these cycles occurred during **slightly more stable** conditions centered near 04 h.*

The identification of these high-stress loading events, and the inflow conditions associated with them, has raised the following questions that will need to be answered in the near future:

- *How often can these large peaks be expected to occur?*
- *What are the appropriate statistical models to describe the distributions of such events?*
- *What are the turbulence conditions associated with them?*
- *Can such inflow conditions be simulated for use by dynamic simulation codes such as* ADAMS® *(Automated Dynamic Analysis of Mechanical Systems)?*

The Need for Stochastic 3-D Turbulence Simulation

Events such as those described above are impossible to simulate using only the longitudinal (u) component of the wind even if it is stochastic. A *full-vector* or three-dimensional simulation is required that includes not only spatial coherence but local cross-axis correlation as well. The latter is needed to simulate the dynamic shearing stress fields observed in actual flows. It is not clear which fluid dynamics parameter or parameters are the best indicators of the coherent turbulence that is responsible for the increased dynamic loading of wind turbines. We hope to answer this question in the near future with further analysis and field measurements.

We have used the computational kernel of the SNLWIND Code developed by Paul Veers of Sandia National Laboratories [1] as a basis for achieving a full-vector simulation. The objective of this work has been to develop the ability to simulate a *statistically relevant* ten-minute record of the three-dimensional wind field found in and near a large wind farm. This simulation also includes, at least statistically, the temporal and spatial variations of coherent structures embedded in the more random inflows found in these locations.

The modeling of the turbulent inflows upwind, downwind, and within a large wind farm was based on extensive measurements taken at a large wind farm in San Gorgonio Pass in southern California [2,3,4]. The methodology used to expand the SNLWIND Code to a full-vector simulation included:

- *Identifying suitable homogeneous terrain spectral models for each of the three wind components (u,v,w) for use as references*
- *Developing empirical "target" velocity spectral scaling based on the measurements taken in San Gorgonio*
- *Developing empirical relationships for the vertical coherence of the longitudinal (u) and crosswind (v) wind components*
- *Deriving empirical relationships between the normalized cross-axis correlations (r_{ij}) and boundary layer scaling parameters*

We used the homogeneous (smooth) terrain models of Olesen, Larsen, and Højstrup [5] as target spectra references. Local spectral scaling was accomplished by applying empirically derived ratios to the appropriate homogeneous terrain model. It was necessary to include up to three spectral peaks to describe the observed 10-minute spectral variation distributions. For example, to describe the crosswind (v) spectra downwind of the wind farm under *unstable* flows three peaks were required: $S_V(n) = S_L(n) + S_H(n) + S_{wake}(n)$. Here, the total spectrum is composed of low-frequency, high-frequency, and turbine wake contributions. The predicted crosswind (v) spectra for a mean hub-height wind speed of 12 ms^{-1} are plotted in Figure 7 for representative unstable, near-neutral, and stable conditions.

The spatial coherence was introduced using an exponential decay model using empirically derived coherence decrements based on the measurements upwind and downwind of the San Gorgonio wind farm. It was found that these decrements were monotonic functions of the hub-height mean wind speed. The observed decrements and corresponding linear regressions are plotted in Figure 8 for the horizontal wind components. Empirical normalized cross-axis covariances (r_{ij}) scaled with boundary layer parameters are used to crossfeed the wind components to simulate the observed shear stresses. For example, a reasonable facsimile of the shear stress means and distributions may be accomplished by crossfeeding the u component with only the v and w velocities per the relationship

$$u'(t) = u'(t) + \overline{r_{uv}}\, v'(t) + 2\overline{r_{uw}}\, w'(t).$$

When simulation locations are downwind and within the wind farm, all three wind components must be crossfed to achieve the reasonable replicas of the observed shear stress distributions.

Conclusions

There is strong evidence that coherent turbulent structures ingested by turbine rotors are responsible for the largest peak stresses seen in the flapwise and edgewise bending moments. These interactions produce a coherent (phase specific) response in the rotor and other structural components because of multiple structural modes being excited simultaneously. The most damaging tension stresses occur during boundary layer conditions most likely to support atmospheric wave motions and enhanced turbine wakes. The expanded version of the Veers SNLWIND Code (SNLWIND-3D) provides a much more realistic simulation of the turbulent inflow seen by turbines installed in various locations within a wind farm in complex terrain.

Acknowledgement

This work has been supported by the U.S. Department of Energy under contract DE-AC02-83CH10093.

References

1. Veers, P., "Three-Dimensional Wind Simulation," SAND88-0152, Sandia National Laboratories, March 1988.

2. Kelley, N.D., "An Initial Look at the Dynamics of the Microscale Flow Field within a Large Wind Farm in Response to Variations in the Natural Inflow," SERI TP-257-3591, Solar Energy Research Institute, October 1989.

3. Kelley, N.D. and A.D. Wright, "A Comparison of Predicted and Observed Turbulent Wind Fields Present in Natural and Internal Wind Park Environment," NREL TP-257-4508, National Renewable Energy Laboratory, October 1991.

4. Kelley, N.D., "Full Vector (3-D) Inflow Simulation in Natural and Wind Farm Environments Using an Expanded Version of the SNLWIND (Veers) Turbulence Code," NREL TP-442-5225, National Renewable Energy Laboratory, November 1992.

5. Olesen, H.R., S.E. Larsen, and J. Højstrup, "Modeling Velocity Spectra in the Lower Part of the Planetary Boundary Layer," *Boundary-Layer Meteorology*, Vol. 29, 1984.

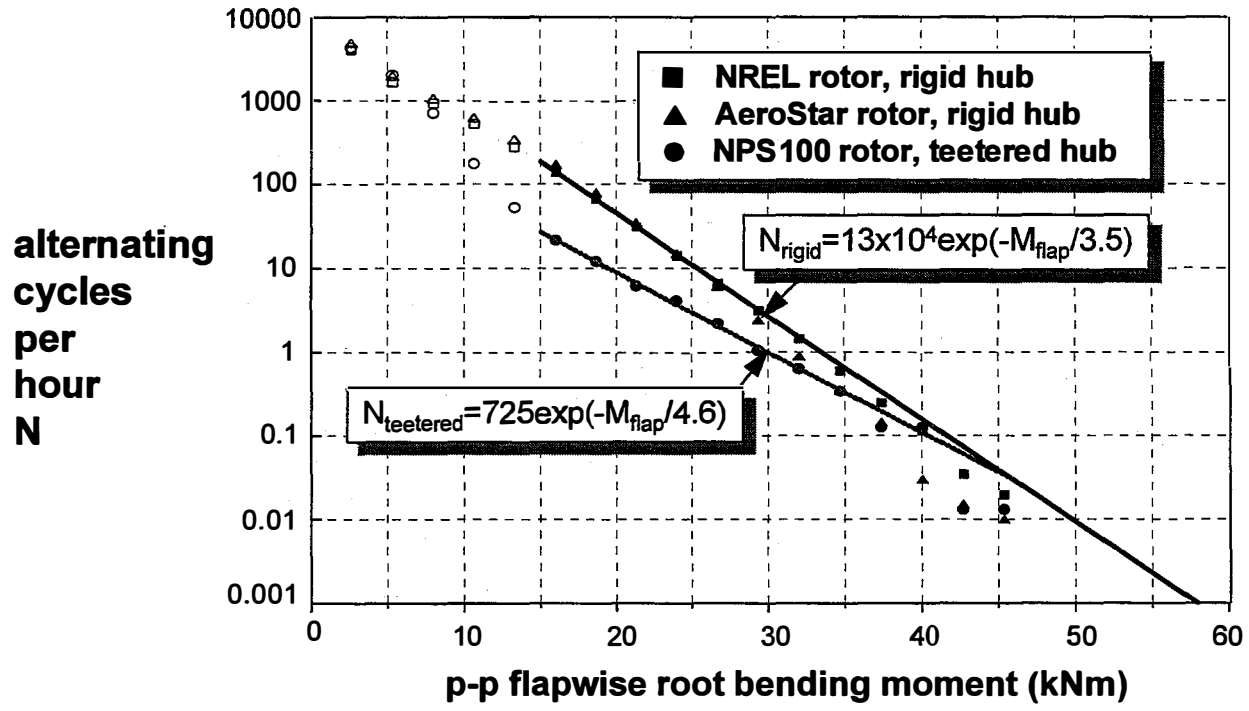

Figure 1. Comparison of rigid- versus teetered-hub low-cycle alternating root flapwise bending loads.

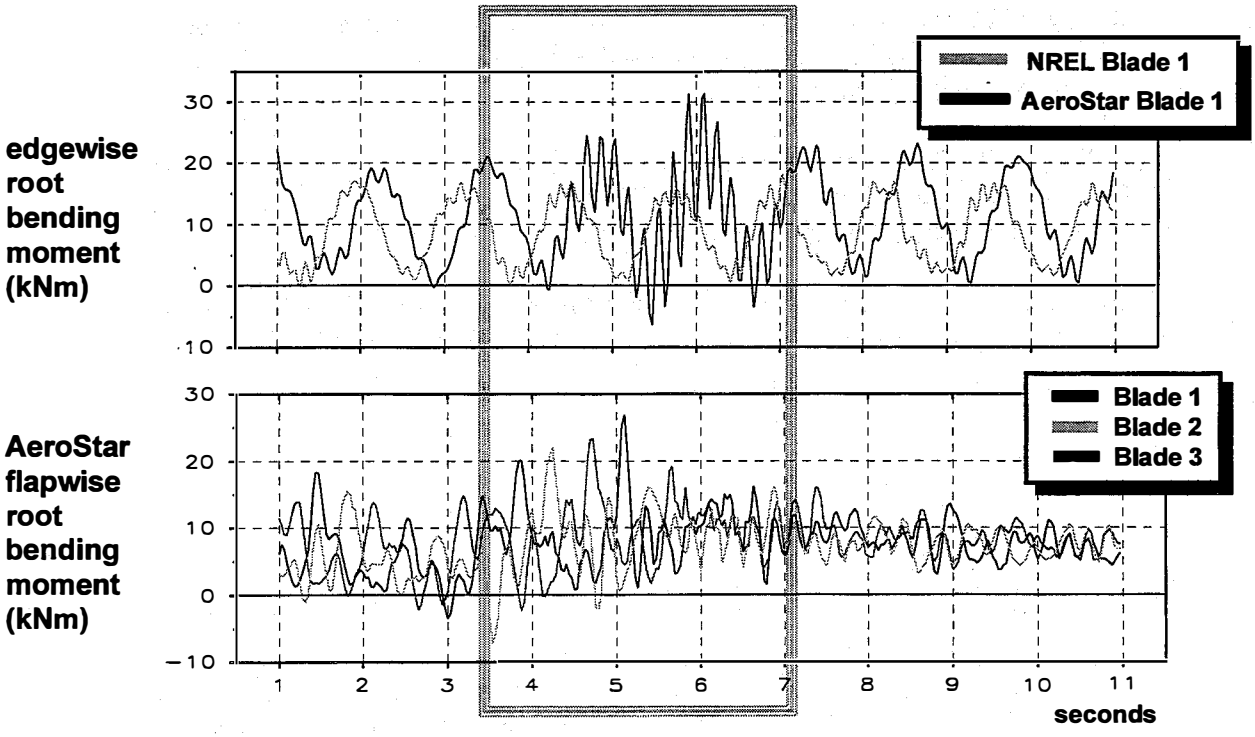

Figure 2. An example of a rotor encountering a coherent turbulent structure.

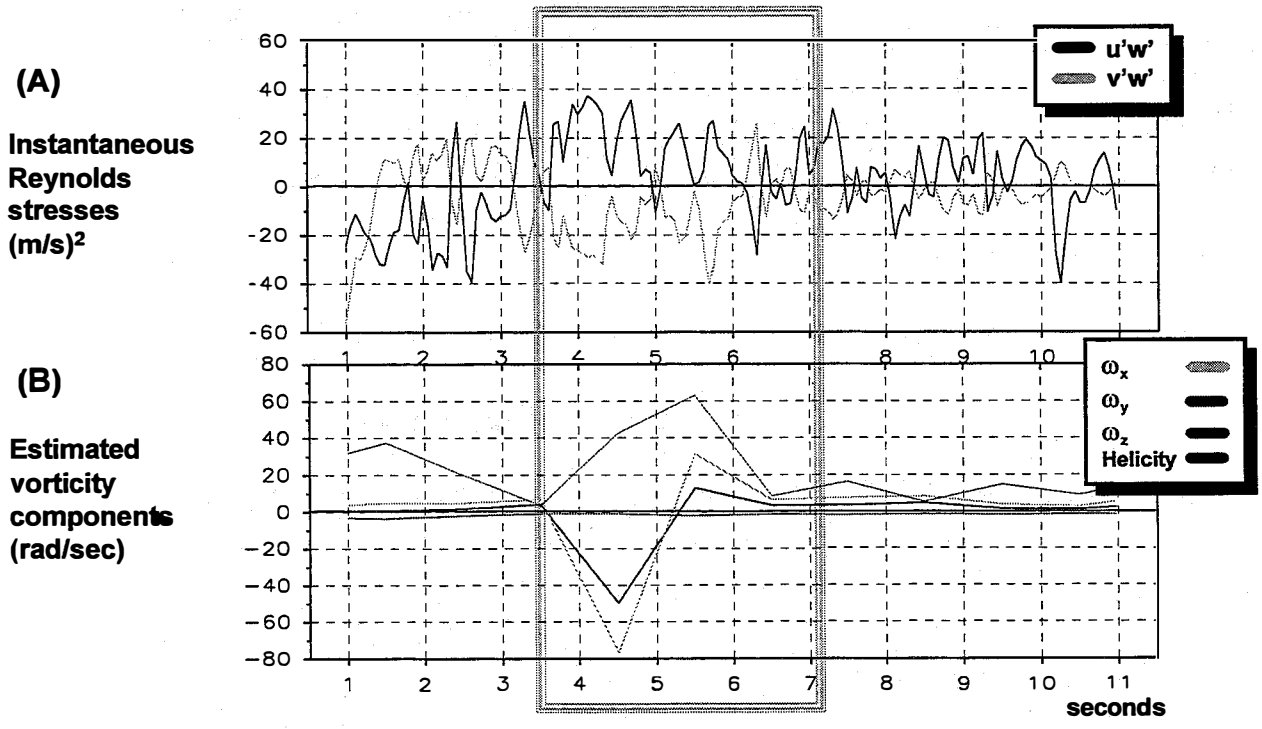

Figure 3. Turbulence characteristics at hub height associated with the response shown in Figure 2.

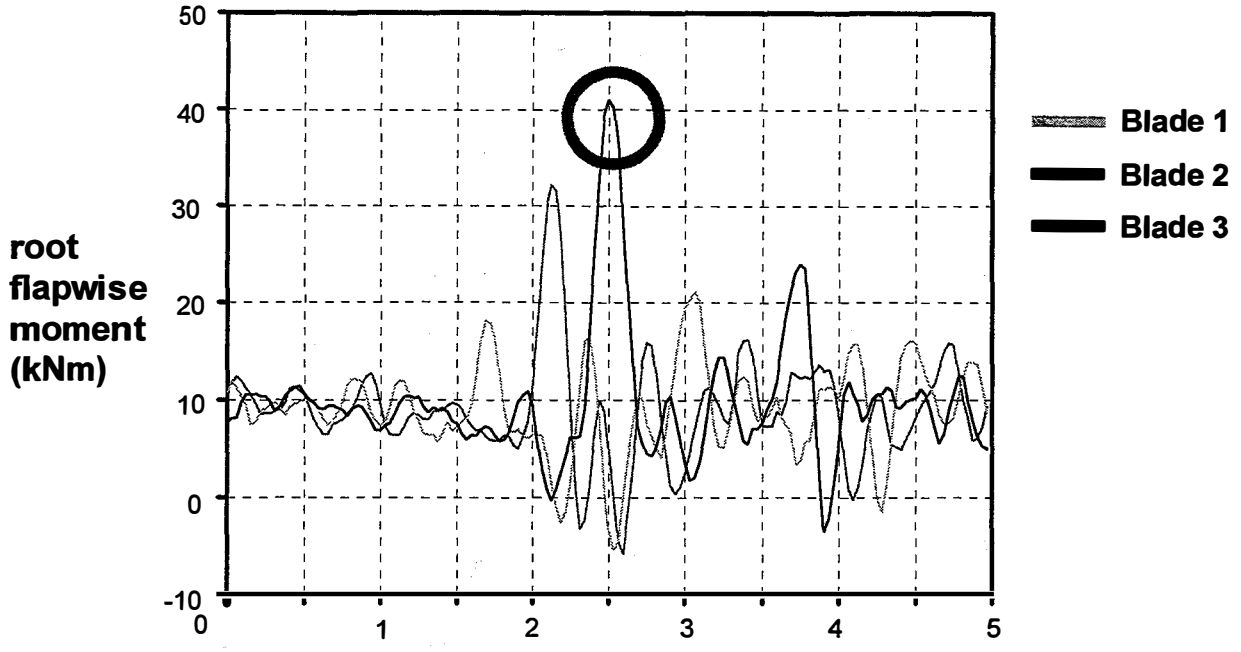

Figure 4a. Largest positive (tension) peak stress cycle observed for the NREL rotor.

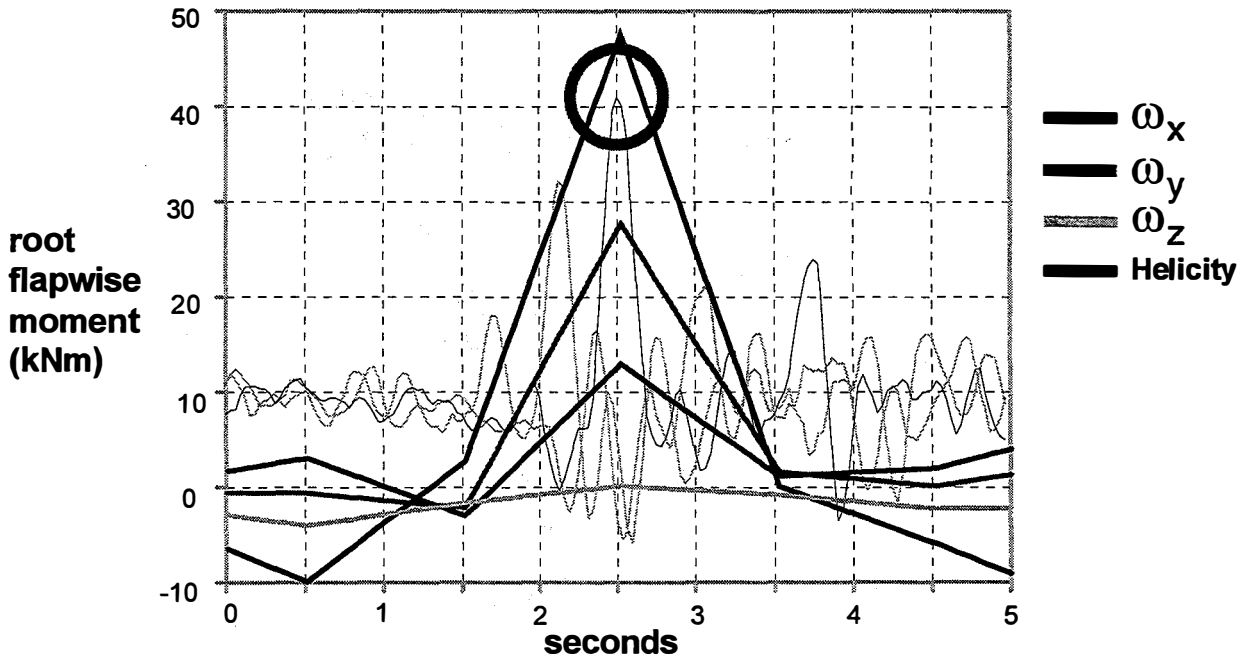

Figure 4b. Hub-height vorticity/helicity estimates aligned with peak flapwise moment.

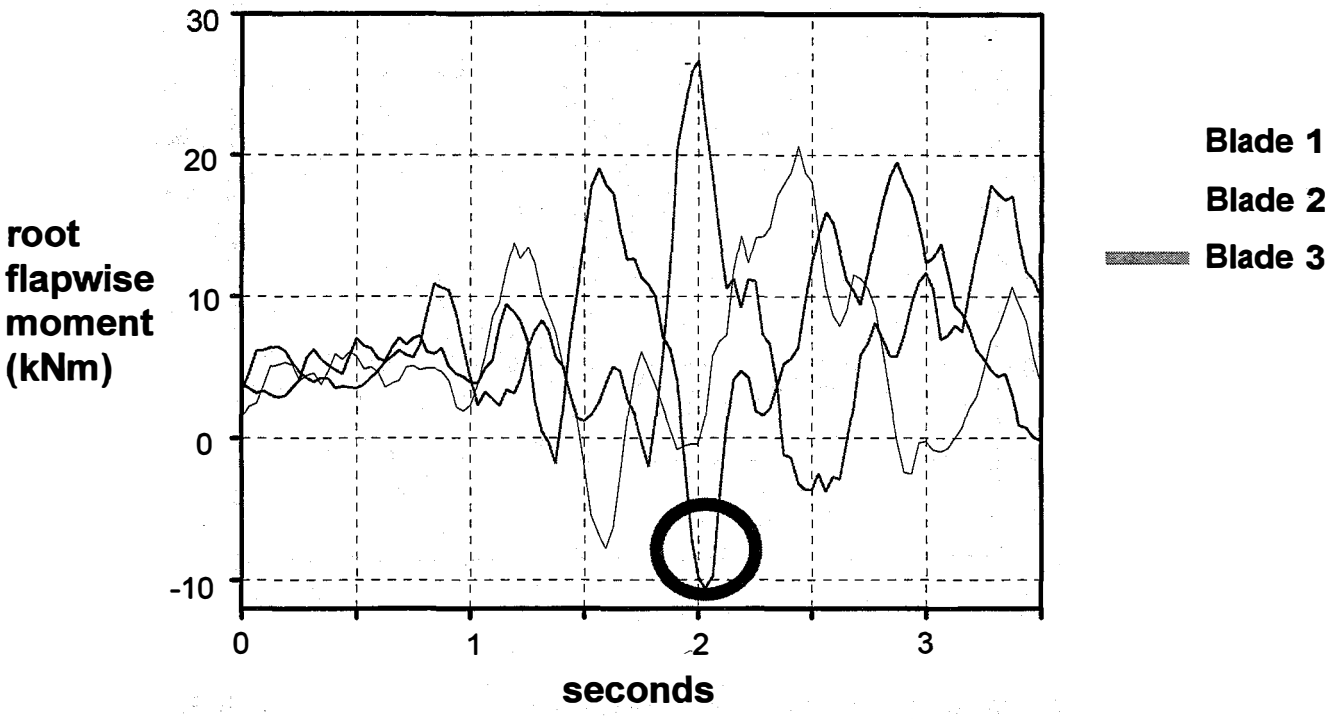

Figure 5a. Large negative (compression) peak stress cycle observed for the NREL rotor.

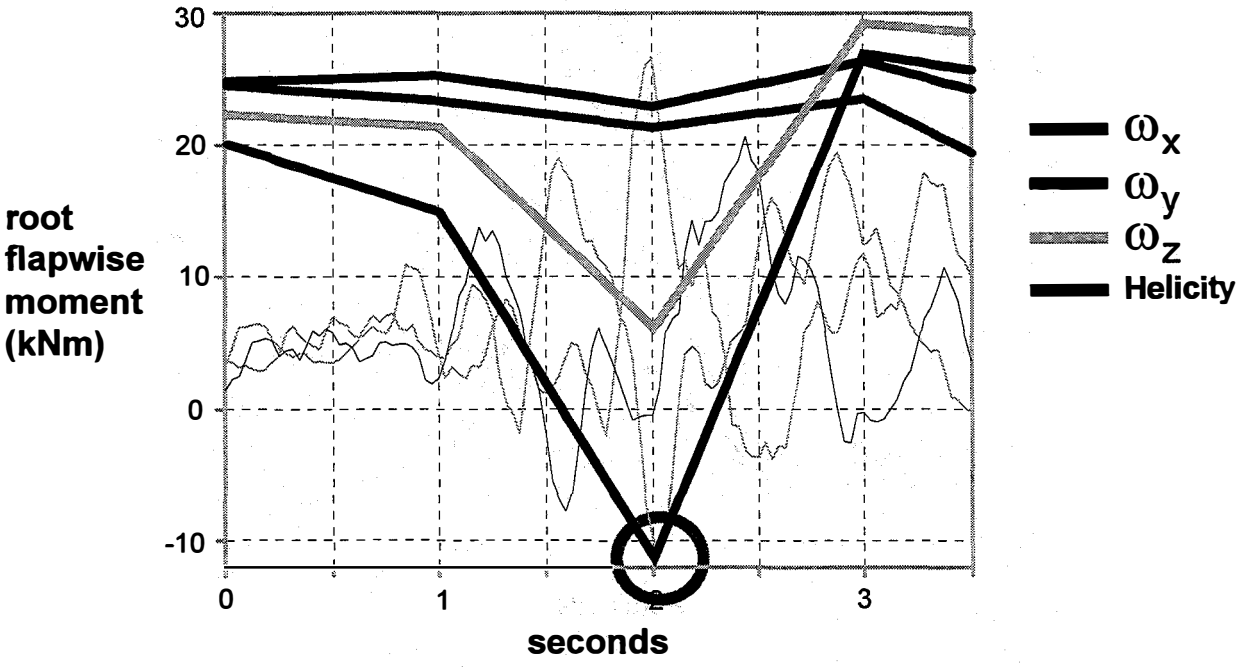

Figure 5b. Hub-level vorticity/helicity estimates overlaid on the record containing the negative peak.

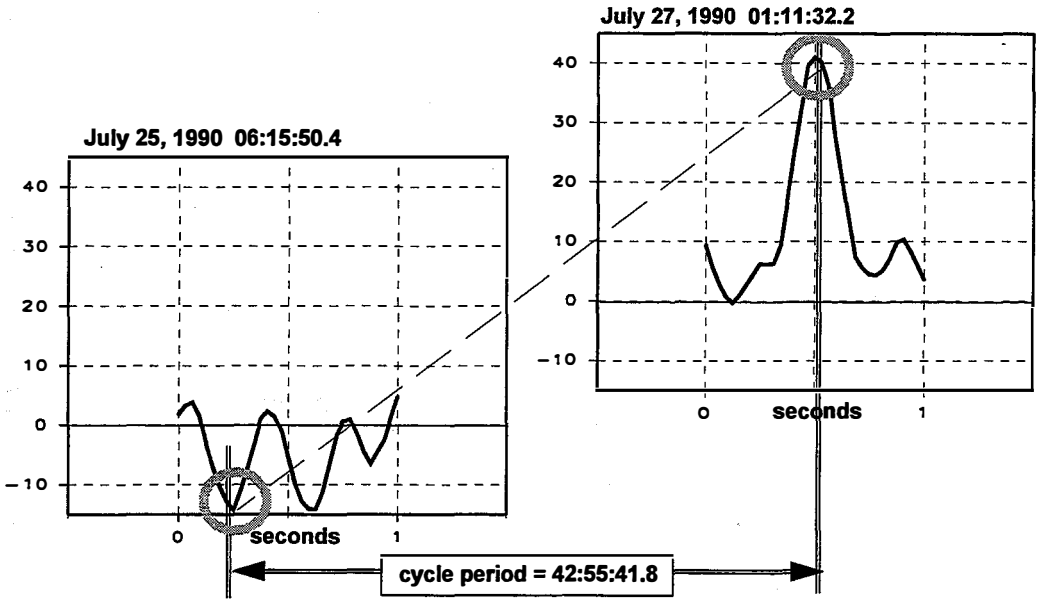

Figure 6. Largest root flapwise bending cycle for the Micon 65 with the NREL rotor.

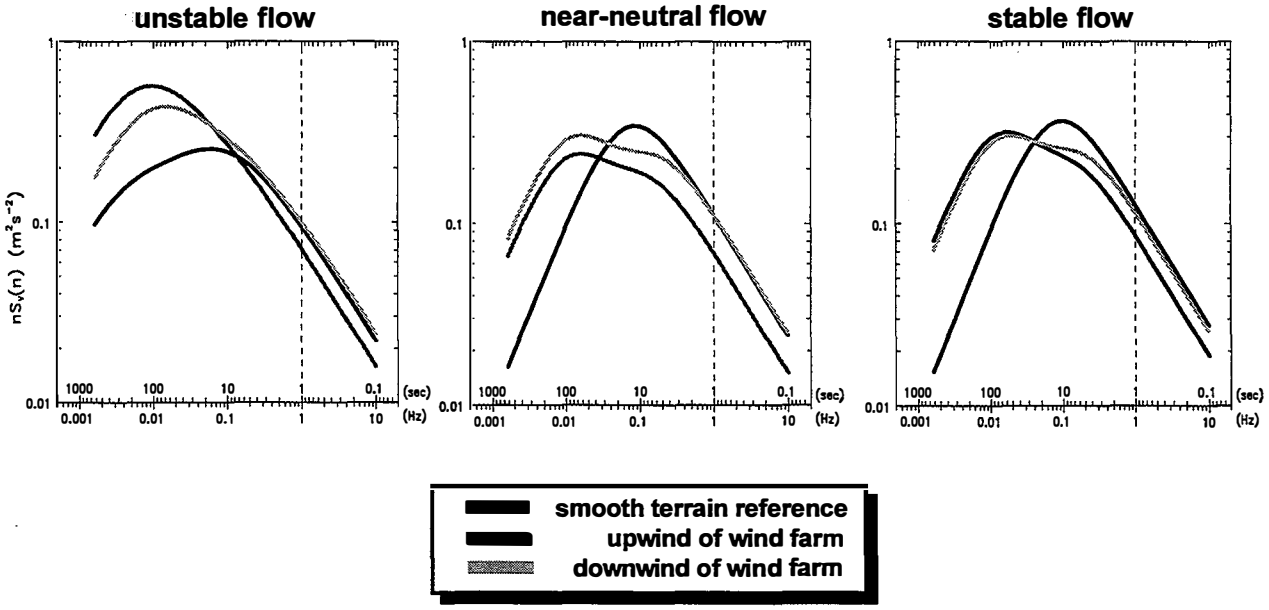

Figure 7. Comparison of predicted crosswind (v) velocity spectra for a 12 ms^{-1} mean wind speed.

Measured Vertical Coherence Decrements

[$Coh^2(n)$]

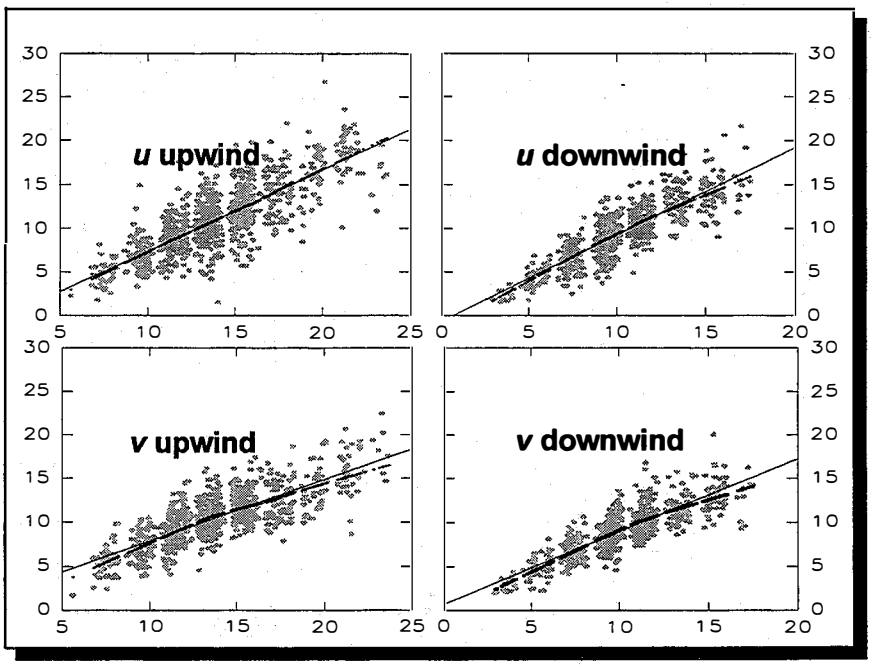

Figure 8. Observed vertical coherence decrements with linear regression lines shown.